Published online 7 October 2015

Nucleic Acids Research, 2015, Vol. 43, No. 19 ***9393–9404***
doi: 10.1093/nar/gkv1010

NPGPx modulates CPEB2-controlled HIF-1α RNA translation in response to oxidative stress

Po-Jen Chen[1], Jui-Yun Weng[1], Pang-Hung Hsu[2], Jin-Yuh Shew[1], Yi-Shuian Huang[3,*] and Wen-Hwa Lee[1,4,*]

[1]Genomics Research Center, Academia Sinica, Taipei 11529, Taiwan, [2]Department of Bioscience and Biotechnology, National Taiwan Ocean University, Keelung, 20224, Taiwan, [3]Institute of Biomedical Sciences, Academia Sinica, Taipei 11529, Taiwan and [4]Graduate Institute of Clinical Medicine, China Medical University, Taichung 40402, Taiwan

Received May 27, 2015; Revised September 22, 2015; Accepted September 23, 2015

ABSTRACT

Non-selenocysteine-containing phospholipid hydroperoxide glutathione peroxidase (NPGPx or GPx7) is an oxidative stress sensor that modulates the antioxidative activity of its target proteins through intermolecular disulfide bond formation. Given NPGPx's role in protecting cells from oxidative damage, identification of the oxidative stress-induced protein complexes, which forms with key stress factors, may offer novel insight into intracellular reactive oxygen species homeostasis. Here, we show that NPGPx forms a disulfide bond with the translational regulator cytoplasmic polyadenylation element-binding protein 2 (CPEB2) that results in negative regulation of hypoxia-inducible factor 1-alpha (HIF-1α) RNA translation. In NPGPx-proficient cells, high oxidative stress that disrupts this bonding compromises the association of CPEB2 with HIF-1α RNA, leading to elevated HIF-1α RNA translation. NPGPx-deficient cells, in contrast, demonstrate increased HIF-1α RNA translation under normoxia with both impaired induction of HIF-1α synthesis and blunted HIF-1α-programmed transcription following oxidative stress. Together, these results reveal a molecular mechanism for how NPGPx mediates CPEB2-controlled HIF-1α RNA translation in a redox-sensitive manner.

INTRODUCTION

Reactive oxygen species (ROS) are natural byproducts of oxygen-dependent cellular reactions, such as the production of superoxide (O_2^-) from mitochondrial respiration and oxidative protein folding in the endoplasmic reticulum (ER) (1,2). ROS are important signaling molecules critical for maintaining homeostasis (3–5). However, cumulative overproduction of ROS can cause macromolecular damage that contributes to a spectrum of physiological disorders or dysfunction, like cancer (6) and aging (7). In an effort to counter this threat, cells have developed many enzymatic redox mechanisms to eliminate excessive ROS. For example, the family of superoxide dismutases initially converts superoxide into hydrogen peroxide (H_2O_2) that is subsequently metabolized to water and oxygen by catalase. Alternatively, thioredoxin peroxidases or glutathione peroxidases (GPx) can reduce H_2O_2 using thioredoxin or glutathione, respectively, as electron donors in the reactions (8–10).

The mammalian GPx family consists of eight phylogenetically related members (GPx1–8) with diverse subcellular distributions. Despite their common action to balance intracellular ROS levels, mouse knockouts of different GPx proteins display a broad range of phenotypic effects (11,12). GPx1 was the first identified and the most abundant GPx (13), but GPx1, GPx2 or GPx3 knockout (KO) mice are viable with grossly normal phenotypes (14–16). Loss of GPx4 or GPx5 results in defective male fertility (17,18). GPx6- or GPx8-deficient mice have not been reported. Of particular interest, GPx7 (i.e. NPGPx) KO mice show systemic oxidative stress, increased tumorigenesis, obesity and shorter life span (19,20). Interestingly, NPGPx does not have enzymatic activity (21,22), but it senses and transmits ROS signaling by transferring the disulfide bonding between its Cys57 and Cys86 residues to downstream effectors, which are involved in obesity, carcinogenesis, protein folding or degradation of non-targeting siRNA stress (19–20,22–26). However, the mechanistic details of how NPGPx alleviates oxidative stress remain to be explored.

HIF-1α is a master regulator for controlling homeostatic responses to hypoxia or various oxidative stresses by activating transcription of many genes important for angiogenesis, metabolism and cell survival (27–29). Interestingly, HIF-1α is constantly synthesized and degraded under normoxic conditions. In response to hypoxia- or chemical-induced oxidative stress, HIF-1α protein levels

*To whom correspondence should be addressed. Tel: +886 22789 8777; Fax: +886 22789 8771; Email: whlee@uci.edu
Correspondence may also be addressed to Yi-Shuian Huang. Tel: +886 22652 3523; Fax: +886 22785 8594; Email: yishuian@ibms.sinica.edu.tw

are rapidly increased by simultaneous blockade of degradation and activation of RNA translation (27–29). Previously, we found that CPEB2 interacts with eukaryotic elongation factor 2 (eEF2) on ribosomes and inhibits guanosine triphosphate hydrolysis activity of eEF2 to negatively regulate HIF-1α RNA translation (30). This mechanism explains the rate-limiting step of HIF-1α RNA translation at elongation instead of initiation (30). Under normoxia, HIF-1α is synthesized at a reduced rate but still undergoes proteasome-mediated degradation. Such an energy-consuming and counterproductive manner of HIF-1α protein synthesis ensures that HIF-1α RNA remains ribosome-associated, thereby facilitating an urgent response to stress. Under increased oxidative stress, the release of CPEB2 from HIF-1α RNA enhances the translation elongation rate of HIF-1α RNA to promptly produce HIF-1α protein (30). However, the underlying mechanism explaining this observation remains to be elucidated.

NPGPx is a critical sensor of oxidative stress. Whether NPGPx plays a role in controlling HIF-1α expression is an open question. In this communication, we found that HIF-1α RNA translation was aberrantly upregulated in NPGPx-deficient mouse embryonic fibroblasts (MEFs) under normoxia. Since CPEB2 is the only RNA-binding protein reported to suppress HIF-1α synthesis under oxygenated conditions (30–32), it is likely that NPGPx modulates HIF-1α RNA translation via CPEB2. Next, we discovered that NPGPx forms a covalent bond with CPEB2 primarily via cysteine residues $C57_{NPGPx}$ and $C157_{CPEB2}$. This interaction promotes a conformational change in CPEB2 and enhances its binding activity to HIF-1α RNA to suppress its translation. In NPGPx-proficient cells, high oxidative stress disrupts this disulfide bonding between NPGPx and CPEB2, which results in an increase of HIF-1α RNA translation. In the absence of NPGPx, HIF-1α RNA translation is already upregulated, yet further induction of HIF1α synthesis is impaired and HIF-1α-programmed transcription is delayed, in response to oxidative stress. Our findings provide a mechanistic framework that links NPGPx and CPEB2 interaction to the regulation of HIF-1α expression as a crucial component of the immediate response to oxidative stress.

MATERIALS AND METHODS

Cell culture, lentiviral infection, transfection and plasmid construction

MEFs were prepared using 13.5-day embryos of the indicated genotypes following the procedures described previously (33). HEK-293T and HeLa cells were cultured in Dulbecco's modified Eagle's medium (DMEM) with 10% fetal bovine serum (FBS). Immortalized human 199Ct fibroblasts were cultured in DMEM/F12 with 10% FBS (34). For reconstituted expression of NPGPx, MEFs were plated in 10-cm dishes to 30% confluence and infected twice with lentiviral particles expressing wild-type (WT) or Cys mutant NPGPx proteins in the presence of 8 μg/ml polybrene. The infected MEFs were selected with 2 μg/ml puromycin and passaged once for further experiments. Transfection of plasmid DNAs was carried out using Lipofectamine 2000 (Invitrogen) following the manufacturer's protocol. The mutants of myc-CPEB2 described herein were generated using the QuikChange Site-Directed Mutagenesis Kit (Stratagene) according to the manufacturer's protocol. The N-terminal mutants of CPEB2 carrying various Cys mutations were transferred to the Ms2CP plasmid for the tethered reporter assay (30). The other plasmid constructs were described previously (19,30).

Sucrose density gradient for polysome profiling

The procedures for performing this analysis were as described (30).

RNA extraction, cDNA synthesis and quantitative PCR (qPCR)

Total RNAs from MEFs were extracted using the TRIzol reagent (Invitrogen). One microgram of total RNA was reverse-transcribed into cDNA and then 1/25 of the cDNA reactions were used for qPCR. The primers used for qPCR are mHIF-1α, 5′-TGGCAGCGATGACACAGAAA-3′ and 5′-AGTGGCTTTGGAGTTTCCGA-3′; hHIF-1α, 5′-TTCCTTCTCTTCTCCGCGTG-3′ and 5′-ACTTATC TTTTTCTTGTCGTTCGC-3′; mGAPDH, 5′-AAGGG CTCATGACCACAGTC-3′ and 5′-CAGGGATGATG TTCTGGGCA-3′; hGAPDH, 5′-GAAAGCCTGCCGG TGACTAA-3′ and 5′-GCCCAATACGACCAAATCA GAG-3′; mVEGF, 5′-CTGGACCCTGGCTTTACTG C-3′ and 5′-TGAACTTGATCACTTCATGGGACT-3′; mGLUT-1, 5′-TCTTAAGTGCGTCAGGGCGT-3′ and 5′ -GTCACCTTCTTGCTGCTGGGA-3′; mHKII, 5′-GCC TCGGTTTCTCTATTTGGC-3′ and 5′-ATACTGGTC AACCTTCTGCACT-3′; m18S, 5′-TGGTTGATCCTGC CAGGTAGCA-3′ and 5′-AGCGACCAAAGGAACCA TAACTGA -3′.

Luciferase reporter assay

MEFs transfected with the DNA mixture containing 1 μg WT or C3A3 myc-CPEB2 plasmid, 1 μg firefly luciferase and 0.5 μg *Renilla* luciferase reporter plasmids, or 293T cells transfected with the DNA mixture containing 0.3 μg WT or C2A2 NPGPx plasmid, 0.3 μg WT or various Cys-to-Ala mutant CPEB2N-Ms2CP, 0.3 μg firefly luciferase and 0.1 μg *Renilla* luciferase reporter plasmids, were harvested and analyzed using Dual-Luciferase Reporter Assay System (Promega).

Immunoprecipitation (IP) and RNA-IP

Immunoprecipitation (IP) was performed as described (19). For RNA-IP, the procedures were as described (30).

Click-iT assay

The assay procedures were as described (30). Briefly, MEFs were incubated with methionine-free medium for 45 min and then metabolically labeled with 50 μM AHA (L-azidohomoalanine). The labeled cells were harvested and the protein concentration was determined by bicinchoninic acid (BCA) protein assay (Pierce). Lysate proteins (100 μg)

were conjugated with biotin-alkyne according to the manufacturer's protocol (Invitrogen), precipitated with Dynabeads M-280 Streptavidin (Invitrogen) and analyzed by immunoblotting.

Western blotting and antibodies

Cells were harvested and lysed with the IP buffer. The lysates were boiled in sodium dodecyl sulphate (SDS) sample buffer (1% SDS, 50 mM Tris–HCl, pH 6.8, 10% glycerol, 50 mM dithiothreitol (DTT) and 0.01% bromophenol blue) and separated by SDS-polyacrylamide gel electrophoresis (PAGE). For non-reducing SDS-PAGE, the lysates were incubated with the sample buffer without DTT at 37°C for 5 min. Antibodies used in this study were NPGPx (cat #GTX70266), green fluorescent protein (GFP, cat #GTX113617) and glyceraldehyde 3-phosphate dehydrogenase (GAPDH, cat #GTX100118) from GeneTex; HIF-1α (cat #NB100–134) from Novus; ribosomal protein S6 (RPS6, cat #74576) from Santa Cruz Biotechnology; FLAG epitope (cat #F1804) from Sigma-Aldrich. CPEB2 and myc antibodies were described previously (30).

Recombinant protein purification and mass spectrum analysis of disulfide bonding interaction

Because recombinant CPEB2 is very insoluble, the small ubiquitin-like modifier (sumo) tag was appended to the N-terminus of CPEB2 to increase the solubility of CPEB2 (35). Recombinant CPEB2 and NPGPx proteins were purified as described previously (19,30). Ten microgram of recombinant NPGPx were incubated with or without 1 μg of recombinant CPEB2 at 25°C for 2 h. The protein mixtures were separated on an 8% non-reducing SDS-PAGE gel, followed by PageBlue staining (Pierce). The protein bands of interest were excised for in-gel digestion with trypsin and chymotrypsin. The resulting peptides were analyzed by tandem mass spectrometry. All MS/MS spectra were converted to the mgf format and analyzed by MassMatrix (http://www.massmatrix.net) according to the previously described procedures (19).

UV-crosslinking RNA-binding and crosslinking-immunoprecipitation (CLIP) assays

The RNA binding assay was performed as described (30). Briefly, the radiolabeled probe of the CPEB2-binding sequence 1904 RNA (36) was mixed with the cell lysates containing myc-CPEB2 proteins and treated with 120 J of UV (254 nm) for 10 min. The UV-treated samples were digested with 200 ng of RNase A at 37°C for 10 min to remove the excess RNA and then analyzed by SDS-PAGE. The corresponding cell lysates were also assayed by immunoblotting to determine the expression level of the myc-CPEB2 variants. The RNA binding activity was calculated based on the amount of the labeled RNA with the total expressed myc-CPEB2 protein.

For the crosslinking-immunoprecipitation (CLIP) assay to measure RNA-binding *in vivo*, the procedure was as described (36). Briefly, the 293T cells expressing full-length, C595A mutant or the N-terminal fragment of myc-CPEB2

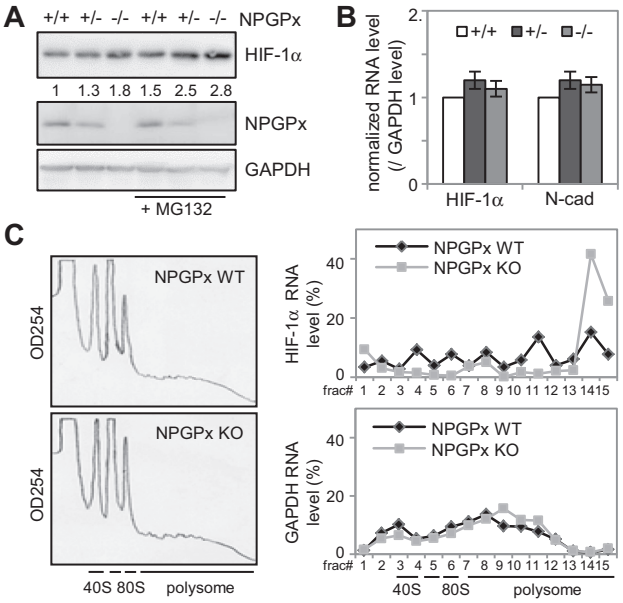

Figure 1. HIF-1α RNA translation is upregulated in NPGPx-deficient MEFs. (**A** and **B**) The NPGPx WT (+/+), heterozygous (+/−) and KO (−/−) MEFs treated or not treated with MG132 for 3 h were harvested for (A) immunoblotting of HIF-1α, NPGPx and GAPDH and (B) RT-qPCR to analyze the levels of HIF-1α and N-cadherin (N-Cad) RNAs (normalized with the GAPDH RNA level). (**C**) Two representative polysome profiles from NPGPx WT and KO MEFs. The polysomal distribution of HIF-1α and GAPDH RNAs in the WT and KO MEFs were determined by RT-qPCR using the RNAs isolated from each fraction.

were incubated overnight with fresh medium containing 50 μM 4-thiouridine. The cells were then irradiated with 120 J of UV (350 nm) for 10 min and harvested for IP using myc IgG-bound magnetic Protein G beads (GE Healthcare Life Sciences). The precipitated samples were treated with calf intestinal phosphatase followed by T4 polynucleotide kinase in the presence of γ-^{32}P-ATP to label the crosslinked RNAs. The samples were then separated by SDS-PAGE. The radioactive signals were monitored by the phosphorimager Typhoon FLA 4100 system (GE Healthcare).

RESULTS

Elevated HIF-1α RNA translation in NPGPx-deficient MEFs

To test whether the presence of NPGPx affects the expression of the oxidative stress-induced transcription factor HIF-1α, the NPGPx wild type (WT, +/+), heterozygous (+/−) and knockout (KO, −/−) MEFs were treated with or without the proteasome inhibitor MG132 and analyzed by immunoblotting (Figure 1A). An approximately two-fold increase of HIF-1α protein expression was observed in the KO MEFs regardless of MG132 treatment (Figure 1A). To explore how NPGPx affects HIF-1α protein expression, we measured HIF-1α RNA levels in WT, heterozygous and KO MEFs, and found that their HIF-1α RNA expression was similar (Figure 1B). This result suggested that NPGPx did not significantly affect HIF-1α RNA transcription. Next, we performed polysome profiling (Figure 1C, left graphs) and found that the distribu-

tion of HIF-1α, but not GAPDH, RNA was shifted toward polysomes of heavy density (Figure 1C), suggesting that NPGPx deficiency selectively enhances HIF-1α RNA translation.

NPGPx covalently binds to CPEB2

To determine whether NPGPx associates specifically with HIF-1α RNA, HEK293T cells expressing HA-tagged WT ($NPGPx^{WT}$) or mutant ($NPGPx^{C2A2}$) NPGPx, whose Cys57 and Cys86 are substituted with Ala to abolish its ability to form disulfide bonds with target molecules (19,25), were used for IP by HA antibody. We found that HIF-1α RNA was present in the immunoprecipitates of $NPGPx^{WT}$ but not $NPGPx^{C2A2}$ (Supplementary Figure S1). NPGPx does not contain a canonical RNA-binding domain to bind RNA directly. It may use its Cys residues to participate in HIF-1α mRNA translation regulation by binding to other factors. Since translation of HIF-1α RNA under normoxia is downregulated by CPEB2 (30), it is likely that NPGPx affects HIF-1α synthesis through CPEB2. We then performed co-IP assays to examine the NPGPx-CPEB2 interaction using 199Ct fibroblast (immortalized primary human fibroblasts) lysates. In the presence of RNase A treatment, NPGPx and CPEB2 were reciprocally co-immunoprecipitated (Figure 2A), suggesting their interaction is RNA-independent. Moreover, when the immunoprecipitates were analyzed by non-reducing (i.e. without the addition of reducing agent DTT) SDS-PAGE, CPEB2 was detected in a high-molecular-weight (HMW) (>130 kDa) complex along with NPGPx, and vice versa (Figure 2B). To ensure the HMW complex was composed of CPEB2 and NPGPx, we ectopically expressed myc-CPEB2 and HA-NPGPx in 293T cells for co-IP assay using HA and myc antibodies. Similarly, HA-NPGPx and myc-CPEB2 were reciprocally associated in the HMW complex, which could be disrupted by DTT (Figure 2C), indicating the interaction between NPGPx and CPEB2 is mediated by disulfide bonding. Furthermore, when we co-transfected, respectively, either $NPGPx^{WT}$ or $NPGPx^{C2A2}$ with myc-tagged CPEB2 (myc-CP2) in 293T cells, only WT, but not mutant, NPGPx was co-immunoprecipitated with CPEB2 (Figure 2D), supporting the conclusion that the CPEB2–NPGPx interaction is mediated by disulfide bonding.

Loss of NPGPx compromises CPEB2-mediated inhibition of HIF-1α RNA translation

CPEB2 has been shown to slow down *de novo* translation of HIF-1α through binding to the HIF-1α RNA 3′-untranslated region (UTR) (30). It is likely that NPGPx may affect CPEB2-controlled translation through this mechanism. To test this possibility, we co-transfected the enhanced GFP (EGFP) reporter appended with the HIF-1α 3′-UTR along with the EGFP-Ms2CP control plasmid (i.e., EGFP is fused with the dimeric bacteriophage Ms2 coat protein to be separated distinctly from EGFP on the gel) into NPGPx WT and KO MEFs for measuring new protein synthesis rate. As shown in Figure 3A, the newly synthesized rate of EGFP, but not EGFP-Ms2CP, was faster in the NPGPx-deficient MEFs (Figure 3A), suggesting that NPGPx affects the translational process mediated by the HIF-1α 3′-UTR. Next, we performed a reporter assay using firefly luciferase (FLuc) appended with the HIF-1α 3′-UTR, along with *Renilla* luciferase (RLuc) to normalize variation in transfection efficiency, in NPGPx WT and KO MEFs upon expression of myc-CPEB2. As shown in Figure 3B, the expression of myc-CPEB2 in NPGPx WT cells significantly suppressed FLuc synthesis, but not in KO MEFs. However, suppression was observed when KO MEFs stably expressing ectopic $NPGPx^{WT}$, but not $NPGPx^{C2A2}$ (Figure 3B). In addition, an RNA-IP assay demonstrated that the association of CPEB2 and HIF-1α RNA was impaired in NPGPx KO MEFs, in contrast to the N-cadherin (N-Cad) RNA non-target control (Figure 3C). These results indicate that NPGPx negatively modulates HIF-1α RNA translation through the 3′-UTR-bound translational repressor CPEB2.

Identification of the cysteine residue(s) in CPEB2 necessary for the interaction with NPGPx

To determine which cysteine residues of CPEB2 responsible for the disulfide bond-mediated interaction with NPGPx, recombinant CPEB2 and NPGPx proteins were combined *in vitro* with or without DTT. The mixtures were then separated by SDS-PAGE and analyzed by PageBlue staining and immunoblotting. As shown in Figure 4A, CPEB2 formed a complex (denoted as band 1) with NPGPx under non-reducing conditions. NPGPx in the band 2 region was also detected in the absence of CPEB2 (Figure 4A). Both bands were processed and analyzed by mass spectrometry. A disulfide linkage between Cys57 of NPGPx and Cys157 of CPEB2 was identified in band 1 (Figure 4B, the mass spectrum in Supplementary Figure S2A). In addition, an intramolecular disulfide bond between Cys444 and Cys595 in the RRM2 segment of CPEB2 (Figure 4C) was also detected in both complexes (Figure 4B, the mass spectrum in Supplementary Figure S2B).

Based on the mass spectrometry data, the Cys157 residue of CPEB2 appeared to be responsible for the binding to NPGPx. To confirm this possibility, 293T cells expressing full-length (myc-CPEB2), N-terminus (myc-CP2N, a.a. 1–456) or C-terminal RNA-binding domain (RBD, myc-CP2C, a.a. 457–716) CPEB2 constructs along with NPGPx were used for co-IP assays with NPGPx antibody. As expected, only the full-length and N-terminus recombinant proteins interacted with NPGPx (Supplementary Figure S3). Sequence alignment of CPEB2 from several species also revealed significant conservation among a cluster of three cysteine residues (Cys157, 350, 444) in the N-terminus of CPEB2 (Figure 5A). Of note, Cys350 is located in the alternatively spliced exon 4. Next, we generated myc-CPEB2 mutants with alanine substitutions at the indicated cysteine sites, including C157A, C350A, C444A, C157/350A, C157/444A, C350/444A and C157/350/444A (C3A3), for testing binding to NPGPx by co-IP. We found that C157 is the most critical residue for disulfide bonding with NPGPx (Figure 5B). Nevertheless, it was noted that substitution of all three Cys residues in the N-terminus of CPEB2 is required to completely abolish the binding to NPGPx (Figure 5B). The NPGPx-binding ability of these CPEB2

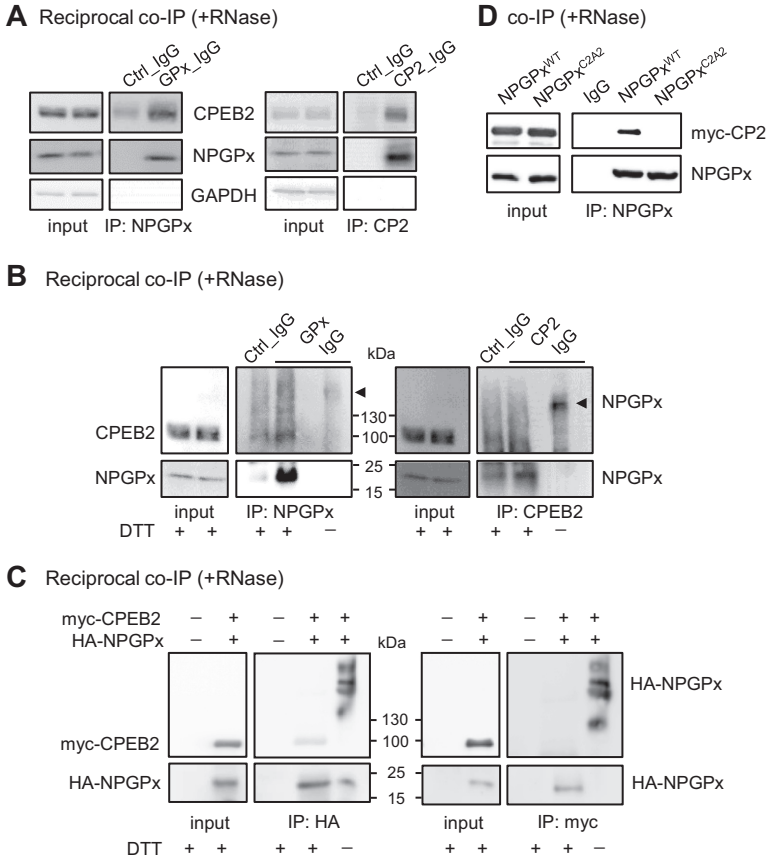

Figure 2. NPGPx covalently associates with CPEB2 via its Cys residues. (**A**) Reciprocal co-immunoprecipitation (co-IP). The immortalized human 199Ct fibroblast lysates treated with RNase A were immunoprecipitated with control (Ctrl), NPGPx (GPx) or CPEB2 (CP2) IgG. The precipitated substances were used for Western blotting of CPEB2, NPGPx and GAPDH. (**B**) The immunocomplexes pulled down by NPGPx or CPEB2 antibody were analyzed by western blotting under reducing (+DTT) or non-reducing (−DTT) conditions. Under the non-reducing condition, a high-molecular-weight complex (denoted by arrowheads) was immunodetected by NPGPx and CPEB2 antibodies. (**C**) The 293T cells expressing myc-CPEB2 and HA-NPGPx were lysed and precipitated with HA or myc antibody, followed by immunoblotting with myc or HA antibodies under ± DTT. (**D**) The 293T cells expressing myc-CPEB2 along with WT ($NPGPx^{WT}$) or C2A2 mutant (C57/86A, $NPGPx^{C2A2}$) of NPGPx were lysed and precipitated with NPGPx antibody, followed by immunoblotting using myc or NPGPx antibodies.

mutants correlated with the amount of HMW complex and oxidized form of CPEB2 detected in the non-reducing SDS-PAGE (Figure 5C). These results suggest that the N-terminal cysteine residues of CPEB2 are important for binding to NPGPx.

Formation of disulfide bonding between NPGPx and CPEB2 is critical for the translational repression activity of CPEB2

To test whether the formation of the covalent bonding with NPGPx is important for the translational repression activity of CPEB2, we expressed the WT and various CPEB2 mutants in cells and compared the amounts of HIF-1α protein in the presence of MG132 by immunoblotting. The CPEB2 C3A3 mutant, which failed to bind to NPGPx (Figure 5B), also did not repress HIF-1α RNA translation (Figure 5D). In contrast, the CPEB2 C2A2 mutants (C157/350A and C157/444A) showed partial binding to NPGPx (Figure 5B) and intermediate inhibition of HIF-1α synthesis (Figure 5D). Expression of these CPEB2 variants did not affect HIF-1α RNA levels (Figure 5D). Similarly, the presence of either the CPEB2 C3A3 (C157/350/444A) or NPGPx C2A2 (C57/86A) mutants was sufficient to abolish CPEB2-suppressed translation of the FLuc-HIF-1α 3′-UTR RNA using the reporter assay (Figure 5E). Although CPEB2 binds to eEF2 via its N-terminus (30), none of these CPEB2 C2A2 and C3A3 mutants were defective in association with eEF2 (Figure 5F). When the N-terminus of CPEB2 (CP2N) carrying either the C2A2 or C3A3 mutations fused to Ms2CP (i.e., a bacteriophage RNA-binding protein that recognizes the unique stem-loop Ms2 sequence) was used in the tethered function assay (30), all of these CP2N-Ms2CP mutants were able to repress FLuc reporter activity (Figure 5G). Thus, the NPGPx–CPEB2 covalent interaction affects the function of the C-terminal RBD of CPEB2, which is critical for CPEB2-controlled translational repression.

Interaction of NPGPx with CPEB2 at its N-terminal cysteine residues affects the C-terminal RNA-binding domain activity

Oxidative stress causes the dissociation of CPEB2 from HIF-1α RNA, resulting in augmentation of HIF-1α syn-

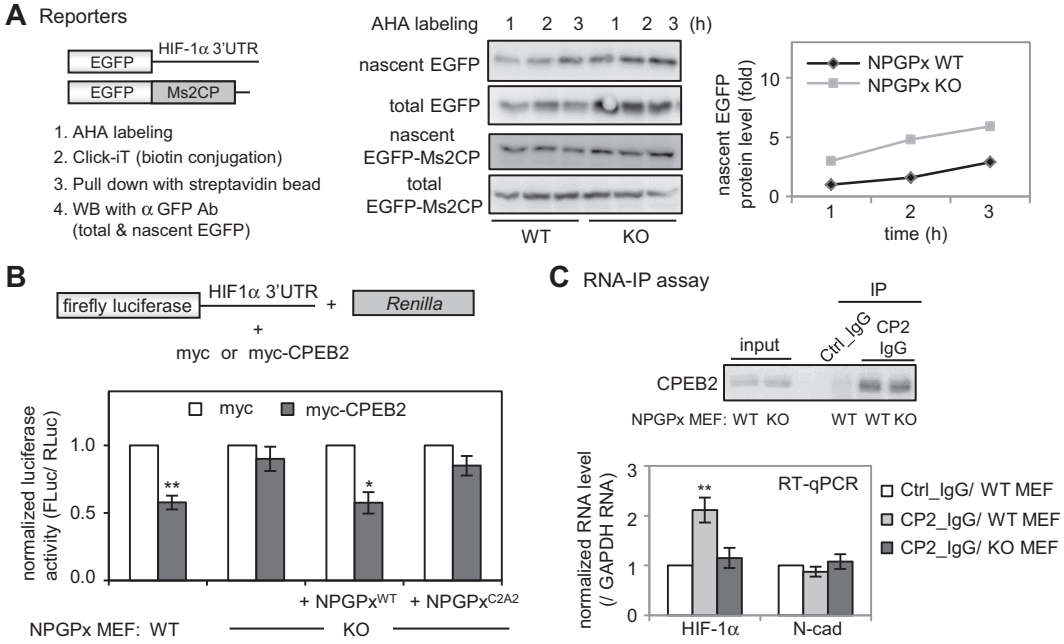

Figure 3. NPGPx is required for CPEB2-inhibited HIF-1α RNA translation. (**A**) The NPGPx WT and KO MEFs transfected with the plasmids encoding EGFP reporters appended without (EGFP-Ms2CP) or with HIF-1α 3′-UTR were metabolically labeled with AHA to tag newly synthesized proteins. EGFP and EGFP-Ms2CP from total cell lysates and the streptavidin-precipitated AHA-labeled proteins were immunodetected by EGFP antibody. The nascent EGFP signals were quantified, expressed as a relative ratio and plotted against time. (**B**) The NPGPx WT, KO and KO MEFs reconstituted with the ectopic expression of $NPGPx^{WT}$ or $NPGPx^{C2A2}$ were transfected with the combination of plasmids expressing firefly (FLuc) and Renilla (RLuc) luciferase reporters along with myc or myc-CPEB2. The cells were harvested for dual luciferase assay. The data from three independent experiments were expressed as mean ± SEM. (**C**) The NPGPx WT and KO MEFs were used for RNA immunoprecipitation (RNA-IP). The control (Ctrl) and CPEB2 (CP2) IgG-precipitated substances were analyzed for the levels of HIF-1α and N-cadherin (N-Cad) RNAs using RT-qPCR with the non-target control GAPDH RNA as the reference. One and two asterisks denote significant difference, $P < 0.05$ and $P < 0.01$, respectively (Student's *t*-test).

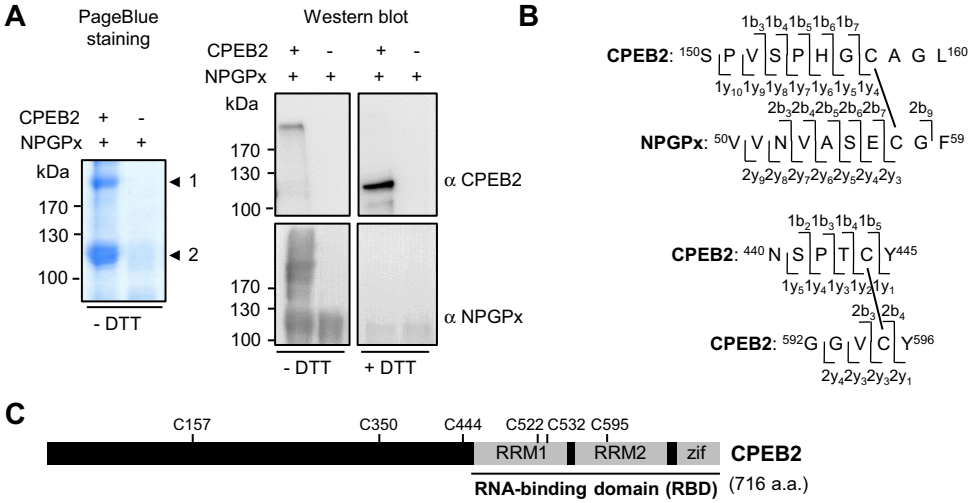

Figure 4. Identification of disulfide-linked residues between NPGPx and CPEB2. (**A**) The reaction mixtures containing recombinant NPGPx with ± recombinant CPEB2 were separated by SDS-PAGE under non-reducing and reducing conditions. The gels were then processed by PageBlue staining or immunoblotting with CPEB2 and NPGPx antibodies. (**B**) The two CPEB2-containing complexes (arrowheads) in (A) were isolated and subjected to mass spectrometry analysis. The identified disulfide bonds, $C57_{NPGPx}$-$C157_{CPEB2}$ and $C444_{CPEB}$-$C595_{CPEB2}$, are schematically presented. (**C**) The C-terminal RNA-binding domain (RBD) in CPEB2 is composed of two RNA recognition motifs (RRM) and two zinc fingers (Zif). Except for those cysteines (C654, 657, 662, 671, 676, 681, 684) in the Zif domain, the relative positions of the other Cys residues in CPEB2 are labeled.

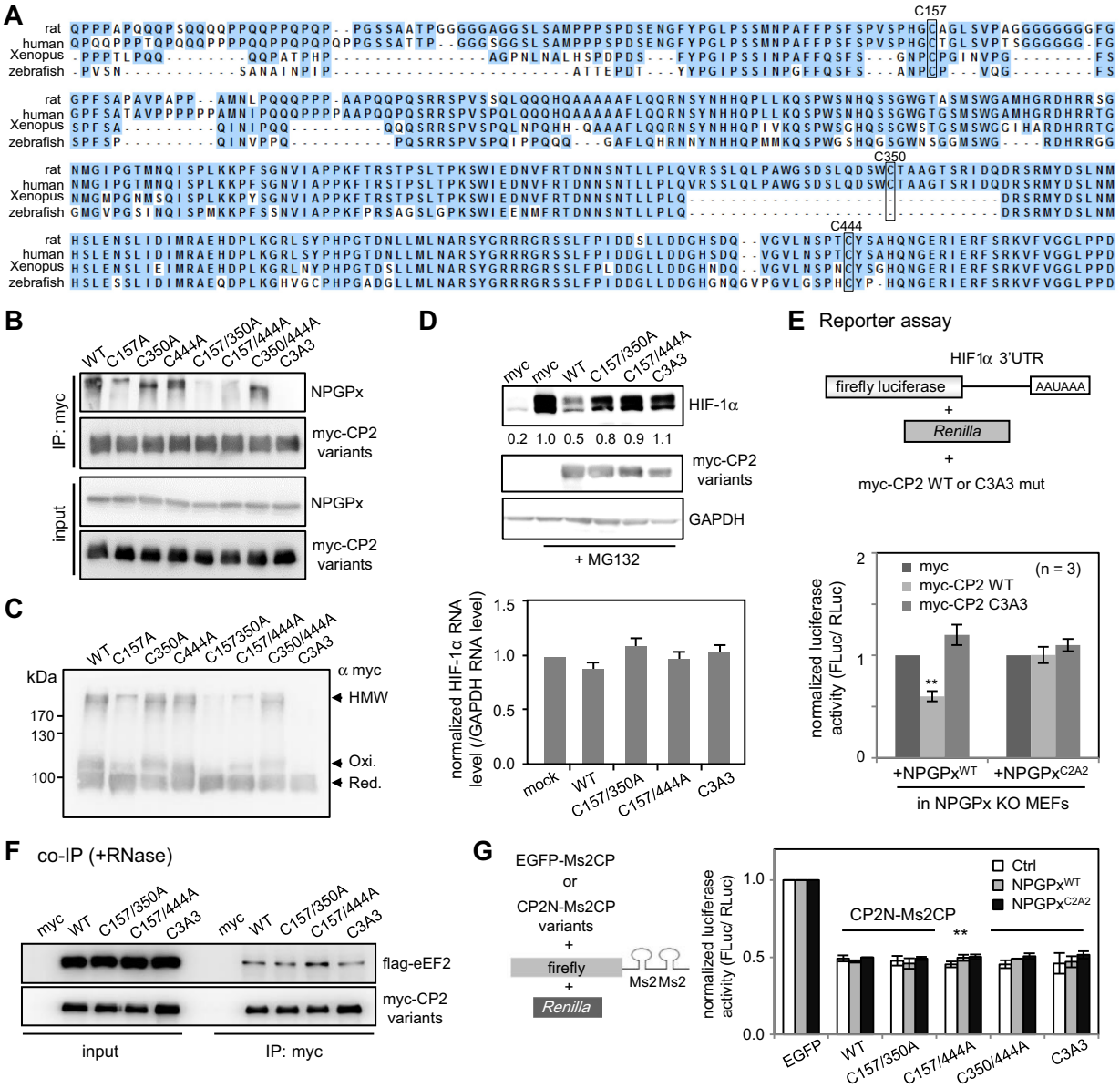

Figure 5. CPEB2 inhibited HIF-1α RNA translation depending on its covalent interaction with NPGPx. (**A**) Alignment of the N-terminal CPEB2 sequences from four vertebrates. The cysteine residues, C157 and C444, in rat CPEB2 are conserved in other species. The C350 residue is located in the alternatively spliced exon 4. (**B** and **C**) The 293T cells expressing myc-tagged WT or various Cys-to-Ala mutants of CPEB2 were used for immunoprecipitation with myc antibody. The immunoprecipitates were either used for (B) immunoblotting with NPGPx and myc antibodies or (C) separated by non-reducing SDS-PAGE to detect high-molecular-weight (HMW), oxidized (Oxi.) and reduced (Red.) forms of myc-CPEB2 variants. (**D**) HeLa cells overexpressing WT or mutant myc-CPEB2 were treated with 20 μM MG132 for 4 h and then harvested for immunoblotting or RT-qPCR to analyze the protein and RNA levels of HIF-1α. (**E**) The NPGPx KO MEFs reconstituted with $NPGPx^{WT}$ or $NPGPx^{C2A2}$ were transfected with the firefly luciferase (FLuc) with HIF-1α 3′-UTR and *Renilla* luciferase (RLuc) along with myc, myc-CPEB2 or myc-C3A3 mutants. The cell lysates were harvested for dual luciferase assay. (**F**) The 293T cell lysates containing flag-eEF2 and WT or mutant myc-CPEB2 were immunoprecipitated with myc antibody. The pull-down substances were used for immunoblotting with flag or myc antibodies. (**G**) Tethered function assay in which either EGFP or the N-terminus of CPEB2 was tethered to the FLuc reporter through a designed interaction between Ms2 coat protein (Ms2CP) and Ms2 stem-loop sequence. The RNA-binding domain of CPEB2 was replaced with the dimeric Ms2CP (CP2N-Ms2CP). EGFP fused with the Ms2CP (EGFP-Ms2CP) was used as a control without any effect on FLuc reporter. The 293T cells transfected with the reporter constructs and the plasmid expressing one of the indicated Ms2CP fusions were analyzed by dual luciferase assay. Error bars in (D, E and G) indicate SEM ($n = 3$). Two asterisks denote significant difference, $P < 0.01$ (Student's *t*-test).

thesis (30). Because the covalent interaction with NPGPx relies mostly on the C157 residue of CPEB2, the formation of the $C57_{NPGPx}$–$C157_{CPEB2}$ linkage likely affects disulfide bonding at the C-terminal RBD to enhance CPEB2 RNA-binding activity. To test this possibility, we used lysates from cells expressing either the WT or C3A3 mutant of CPEB2 for the RNA-IP assay and found less HIF1-α RNA associated with the C3A3 mutant (Figure 6A). Furthermore, when we used cytoplasmic lysates prepared from 293T cells overexpressing WT, the C157/444A mutant or the C3A3 mutant of CPEB2 for a UV-crosslinking RNA-binding assay and immunoblotting to measure RNA-binding activity, the C3A3 mutant was again found to be defective (based on a normalized value reflecting the ratio of RNA-binding signal versus the expression level) (Figure 6B). Apparently, the cysteine mutation at the N-terminus of CPEB2 affects the RNA-binding activity of its C-terminal RBD.

Interestingly, a disulfide link between Cys444 and Cys595 in the RNA recognition motif 2 (RRM2) of CPEB2 was identified (Figure 4B). The interaction of NPGPx–CPEB2 may facilitate the formation of this Cys444–Cys595 bond to alter the RNA-binding activity of CPEB2. We then tested the RNA binding activity of CPEB2 in the presence of DTT and/or with C3A3 mutations, and found that under both conditions, CPEB2 RNA-binding activity was significantly reduced (Figure 6C). However, the addition of C595A mutation in CPEB2 under both aforementioned conditions only moderately decreased RNA-binding activity (Figure 6C). To precisely evaluate the binding activity of the C595A mutant *in vivo*, 293T cells transfected with plasmids expressing the WT, C595A mutant or the N-terminus of CPEB2 were UV-crosslinked and immunoprecipitated. The bound and crosslinked RNAs were subsequently radiolabeled. Using this CLIP approach (37), we found the C595A mutant had ∼20% reduction in RNA binding (Figure 6D). Similarly, the RBD without Cys444 (myc-CP2C) also bound to RNA in a DTT-sensitive manner (Figure 6E). In agreement with the recent structure study in which none of these Cys residues in the RBD was found to be directly in contact with RNA (38,39), the formation of the Cys444-Cys595 bond in CPEB2 likely promotes conformational rearrangement to achieve optimal, but not essential, RNA-binding activity.

Oxidative stress weakens the NPGPx–CPEB2 interaction to initiate HIF-1α expression and HIF-1α-programmed transcription

It was noted that arsenite-induced oxidative stress causes the dissociation of CPEB2 from HIF-1α RNA and consequently upregulates translation of HIF-1α RNA (30). The aforementioned results showed that NPGPx modulates the RNA-binding activity of CPEB2 in a redox-dependent manner. Thus, it is likely that oxidative stress disrupts the NPGPx–CPEB2 covalent interaction and hence weakens the binding of CPEB2 to HIF-1α RNA. To test this possibility, fibroblast cells were treated with H_2O_2 for the indicated times to induce oxidative stress, and reciprocal co-IP/immunoblotting assays with CPEB2 and NPGPx antibodies were performed on the lysates. As shown in Figure 7A, there is decreased interaction between CPEB2 and NPGPx with the increasing duration of H_2O_2 treatment. Similar to arsenite (30), H_2O_2 treatment also abolished the association of CPEB2 and HIF-1α RNA in the RNA-IP assay (Figure 7B). The level of HIF-1α in NPGPx-deficient MEFs was elevated under normoxia; however, H_2O_2-induced HIF-1α synthesis was only evident in the WT MEFs (Figure 7C). Similar results were obtained when the cells were incubated in the 1% O_2 hypoxia chamber (Supplementary Figure S4A).

Since HIF-1α induction was not detected following treatment with H_2O_2 or 1% O_2 of NPGPx KO MEFs, we hypothesized that stress-induced HIF-1α-controlled transcription may be diminished in the absence of NPGPx. To test this possibility, we examined the expression of several HIF-1α target genes in the NPGPx WT and KO MEFs treated with H_2O_2 or 1% O_2. The levels of vascular endothelial growth factor (VEGF), glucose transporter-1 (GLUT-1) and hexokinase II (HK II) RNAs in the WT MEFs were significantly higher than those in the KO cells within 2–4 h of H_2O_2 treatment (Figure 7D) or by 12–24 h of 1% O_2 incubation (Supplementary Figure S4B). Taken together, these results demonstrate a potential mechanism of how NPGPx, in response to cellular redox conditions, modulates CPEB2-controlled HIF-1α RNA translation that is critical for tuning HIF-1α-programmed transcription.

DISCUSSION

The observation that NPGPx KO mice exhibit elevated systemic oxidative stress and shortened life span strongly suggests a critical role of NPGPx in redox homeostasis (19). NPGPx, lacking glutathione-binding and peroxidase activity (22), senses cellular redox status and conveys ROS signaling to its downstream effectors via Cys57 and Cys86 (19,25). The function of the NPGPx-catalyzed thiol-based redox reaction is to enhance the function of its target substrates (19,25) involved in stress defense and the balance of redox status in cells. In this communication, we show that CPEB2 is another cytoplasmic substrate of NPGPx. In addition, we found that the covalent interaction between CPEB2 and NPGPx is important for optimal RNA-binding activity of CPEB2, which is crucial for CPEB2's suppression of HIF-1α RNA translation under normoxia. Such a unique mechanism explains how redox signaling modulates CPEB2-controlled translation.

HIF-1α is a critical factor for hypoxic adaption and embryonic cells lacking HIF-1α exhibit a decreased growth rate under hypoxic, but not normoxic, environmental conditions (40–42). HIF-1α is also known to play essential roles in tumorigenesis and its expression is correlated with cancer prognosis (28,43–44). Specific ablation of *hif-1α* in stromal fibroblasts accelerates mammary tumor growth that is accompanied by a reduction in vascular density and macrophage infiltration (45). Thus, the expression of HIF-1α must be tightly controlled to maintain normal physiological functions. Although NPGPx null mice initially develop normally, the accumulation of oxidative stress damage as they age contributes to a higher occurrence of tumorigenesis and other diseases (19). Consistently, NPGPx was found to protect against oxidative stress-induced DNA damage and reduce the incidence of carcinogenesis (24,46–

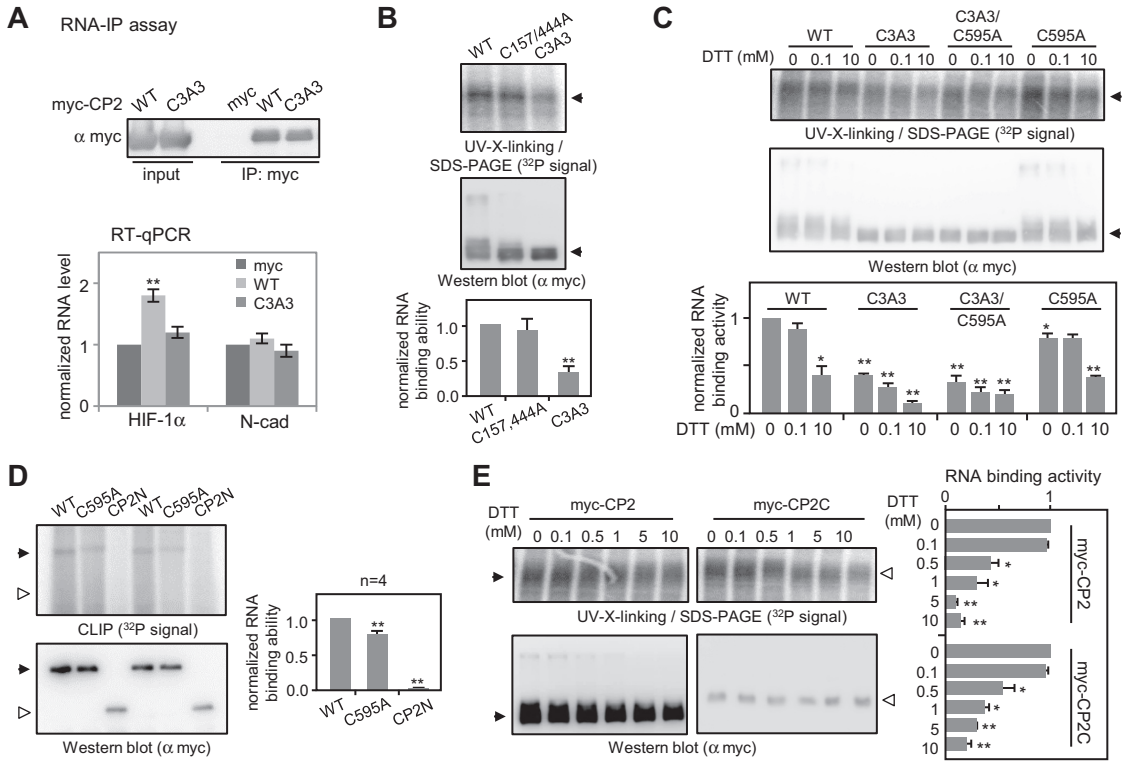

Figure 6. NPGPx-CPEB2 modulates the RNA-binding activity of CPEB2. (**A**) RNA-IP assay. The 293T cells transfected with the plasmids expressing myc-tag, WT or C3A3 mutant of myc-CPEB2 were lysed and immunoprecipitated with myc IgG. The levels of precipitated HIF-1α and N-Cad RNAs were analyzed by RT-qPCR using the amount of GAPDH RNA for normalization. (**B**) The 293T cell lysates containing WT, C2A2 and C3A3 mutant CPEB2 were treated or not treated with DTT of indicated concentration. The cell lysates were UV-cross-linked with ^{32}P-labeled 1904 RNA probe to measure RNA binding or used for immunoblotting. The normalized RNA-binding abilities (the ratio of RNA-binding signal versus the expression level) of various CPEB2 mutants were quantified and expressed as a relative ratio. (**C**) Similar to (**B**), more CPEB2 mutants were tested to measure their RNA-binding abilities. (**D**) *In vivo* RNA-binding assay. The 293T cells expressing WT, C595A and the N-terminus of myc-CPEB2 were UV-irradiated to crosslink the RNA–protein complex *in vivo*. The cells were then lysed and precipitated with myc IgG. The amounts of pull-down proteins were detected by immunoblotting and their associated RNAs were radiolabeled and determined by phosphorimager. Solid and open arrows denoted WT and CP2N signals, respectively. (**E**) The RNA-binding abilities of full-length (solid arrows) and the C-terminal (open arrows) CPEB2 were measured in the presence of DTT. The results from three (A–C and E) or four (D) independent experiments were expressed as mean ± SEM. One and two asterisks denote significant difference, $P < 0.05$ and $P < 0.01$, respectively (Student's *t*-test).

47). Our findings that the loss of NPGPx results in elevated HIF-1α RNA translation under normoxia with delays in HIF-1α-activated transcription under hypoxia and oxidative stress provides a potential link between these two important molecules (Figures 1 and 7). However, whether the aberrant HIF-1α expression in the NPGPx KO mice significantly contributes to tumor formation and other diseases awaits further investigation.

It was shown that several RNA-binding proteins, such as iron regulatory protein 2, chloroplast poly(A)-binding protein, HuR and TAR DNA-binding protein 43, alter their RNA-binding ability via thiol-based redox regulatory processes targeting their RNA-binding domains (48–52). Similarly, NPGPx covalently binds to the N-terminal cysteine residues of CPEB2, subsequently altering the RNA-binding activity of the CPEB2 C-terminal RBD. Although it requires alanine substitution of all three N-terminal cysteines (Cys157, Cys350 and Cys444) in CPEB2 to completely abolish its covalent interaction with NPGPx (Figure 5B and C), Cys157 appears to be the major cysteine to form a disulfide bond with NPGPx (Figures 4 and 5). Intriguingly, the single nucleotide polymorphism (SNP) database shows that the SNP rs373750640 in the *cpeb2* gene causes a missense mutation (C157Y). Based on our results, this substitution would be expected to influence redox signaling-regulated CPEB2-controlled translation. It would be of great interest to further explore whether the C157Y mutation in CPEB2 is linked to other abnormalities or is more prevalent in pathological conditions, including cancers.

All CPEB1 and CPEB1-like proteins (CPEB2, CPEB3 and CPEB4) have a similar structure in which the carboxyl-terminal RBD is composed of two RNA recognition motifs (RRM) and two zinc fingers (Zifs) (Figure 4C). In particular, CPEB2, CPEB3 and CPEB4, which share 96% sequence identity and contain ten cysteine residues (Figure 4C) in the RBD, bind to RNAs with the same sequence specificity *in vitro* (36). Nevertheless, it is not known if CPEBs2–4 bind to the same repertoire of RNAs or exhibit functional redundancy *in vivo*. Similar to CPEB1, several studies indicate that CPEBs2–4 function as activators or repressors in the translational regulation of their target RNAs, but the mechanisms employed by each CPEB to control protein synthesis appear to differ (30,36,53–56). Moreover, why a CPEB functions as an activator for some RNAs but as a

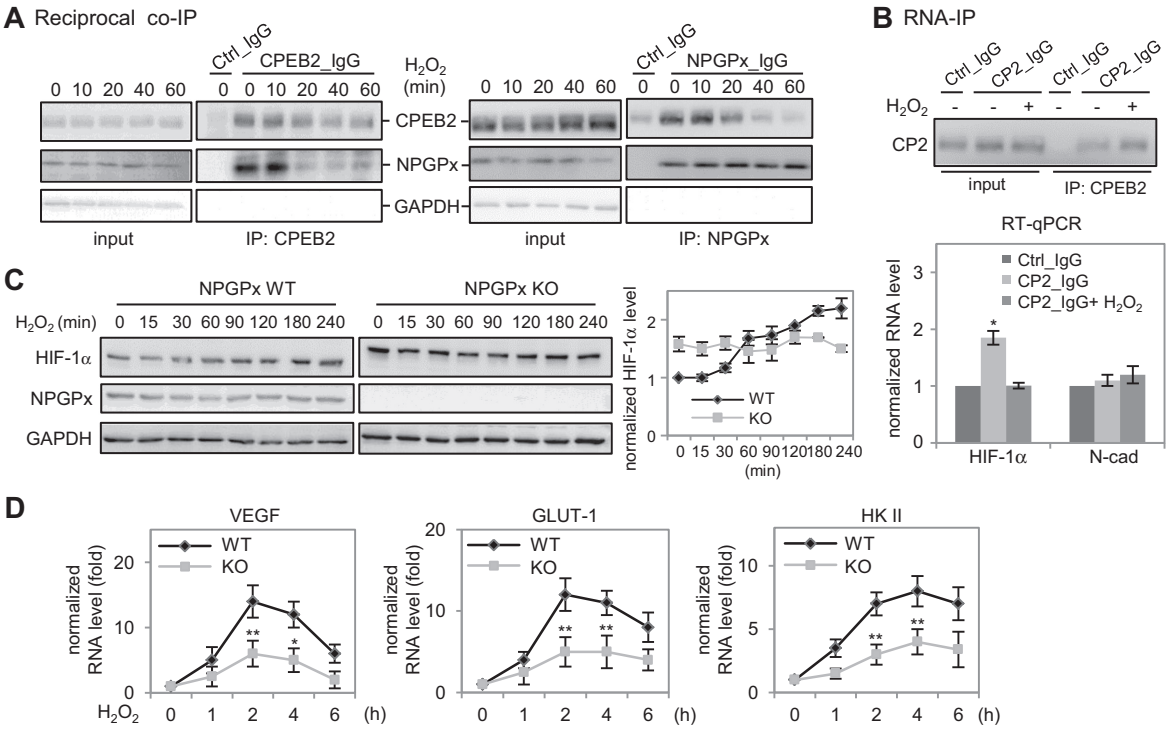

Figure 7. Oxidative stress induces the dissociation of NPGPx–CPEB2 and CPEB2–HIF-1α RNA complexes to upregulate HIF-1α synthesis. (**A**) Reciprocal co-IP assay was performed to analyze the covalent interaction between CPEB2 and NPGPx in the 199Ct fibroblasts treated with H_2O_2 for the indicated duration. (**B**) The control and CPEB2 immunoprecipitates from the 199Ct fibroblasts treated with $\pm H_2O_2$ were analyzed for the amount of HIF-1α and N-Cad RNAs. (**C**) The HIF-1α expression in the NPGPx WT and KO MEFs after the treatment of H_2O_2 for the indicated duration were quantified by immunoblotting and expressed as a relative ratio against time. (**D**) Similarly, the RNAs isolated from the H_2O_2-treated WT and KO MEFs were used for RT-qPCR to determine the VEGF, GLUT-1 and HK II RNA levels (normalized with 18S RNA level). The data from three independent experiments were expressed as mean ± SEM. One and two asterisks denote significant difference, $P < 0.05$ and $P < 0.01$, respectively (Student's *t*-test).

repressor for others remains enigmatic. Despite the presence of all four CPEBs in the hippocampus, studies looking at the effects on hippocampus-related learning and memory in mouse knockout models of the *cpeb1* (57), *cpeb3* (58) or *cpeb4* (59) genes suggest that CPEBs are not functionally redundant *in vivo* as these animals do not phenocopy each other. Although CPEB2 null mice have not yet been reported, we believe for at least two reasons that the NPGPx-regulated RNA-binding mechanism applies only to CPEB2 and not the other CPEBs. First, CPEB3 and CPEB4 contain only one cysteine at the N-terminus, which is located in close proximity to Cys444 of CPEB2 (Supplementary Figure S5A, marked with red rectangles). Second, the high-molecular-weight protein complex was only detected for myc-CPEB2, and not for either myc-CPEB3 or myc-CPEB4, under non-reducing conditions (Supplementary Figure S5B). Thus, the specific covalent interaction between CPEB2 and NPGPx likely makes this aspect of CPEB2-controlled translational regulation unique among all the CPEBs.

The identification of the $C57_{NPGPx}$–$C157_{CPEB2}$ and $C444_{CPEB2}$–$C595_{CPEB2}$ disulfide bonds *in vitro* (Figure 4) raises some interesting issues. The covalent interaction with NPGPx may facilitate CPEB2's formation of an intramolecular disulfide bond between its C444 and C595 residues to enhance its RNA-binding ability. Based on the observations that the RNA-binding activities of the C157/444A and C595A mutants were less affected than the C3A3 (C157/350/444A) mutant (Figure 6B and C) and the activity of all these CPEB2 mutants, like the WT protein, is sensitive to DTT, there is the possibility that disulfide bond formation in CPEB2 can be rearranged dynamically. Although C157 is the key residue covalently linking CPEB2 to NPGPx, the C157A mutant does not completely lose interaction with NPGPx. Similarly, C444 may form alternative disulfide bonds with C522 or C532 in the RRM1 of the C595A mutant protein. It was reported that yeast Gpx3 forms a disulfide bond between its Cys36 and the Cys598 of Yap1 with the thionilate anion formed at Cys303 of Yap1 then attacking this bond to establish the first intramolecular disulfide bond (Cys303–Cys598) in Yap1. Sequentially, the second, third and fourth disulfide bonds linking the N- and C-terminal domains are formed (60). A similar mechanism may apply to the NPGPx and CPEB2 interaction.

Dynamic cysteine-based redox switches are difficult to predict and can only be monitored using nuclear magnetic resonance spectroscopy. Due to the intrinsic insolubility of either the full-length or the C-terminal RBD constructs of all recombinant CPEB proteins, it is difficult to obtain reliable structural information. Although the two RRMs and two Zifs (C4 and C2H2 types) in the RBD of CPEBs were initially thought to be all required for RNA-binding based on reduced RNA-binding in Zif-deleted or Zif-disrupted mutants (36,61), two recent structure studies on RRM1–

RRM2 of CPEB1 and CPEB4 suggest otherwise (38,39). None of the three cysteines in the RRMs of CPEB4 are in direct contact with RNA (i.e. C522, C532, C595 in CPEB2), supporting the notion that disulfide bond formation between C444 and any one of the more C-terminal cysteines is likely to modulate but not determine the binding to RNAs. Based on structure data obtained for the CPEB1 Zif domain (38,62), sequence alignment predicts that CPEBs2–4 also contain C4 and C2H2 Zif motifs (Supplementary Figure S6A). However, an extra cysteine (C657) is present in the Zif domain of CPEB2. Alanine substitution of either C654 or C657 of CPEB2 dramatically decreases the protein's solubility in cells (Supplementary Figure S6B). Thus, it is likely that the extra cysteine in the Zif domain of CPEB2 has an important role in stabilization of CPEB2.

In summary, our findings described here reveal a unique example of how HIF-1α RNA translation is coupled with NPGPx-modulated RNA-binding of CPEB2 to tightly control HIF-1α synthesis in a redox-dependent manner.

SUPPLEMENTARY DATA

Supplementary Data are available at NAR Online.

ACKNOWLEDGEMENTS

We thank Dr Alex Ball for his critical reading of the manuscript and the GRC Mass Spectrometry Facility for the mass spectrum service. We appreciate Jenny Lin, Fang-Yi Su and Ping-kun Hsieh for their kind assistance throughout this study. P.-J.C. performed all experiments except mass spectrum analysis and CLIP assay, which were conducted by J.-Y.W. and Y.-S.H., respectively. P.-J.C., P.-H.H., J-YS, Y.-S.H. and W.-H.L. analyzed the data. P.-J.C., Y.-S.H. and W.-H.L. wrote and completed the manuscript. Y-SH and W.-H.L. supervised the entire study.

FUNDING

Academia Sinica, the Ministry of Science and Technology (MoST) [MoST-103-2321 to W.-H.L.]; National Health Research Institute (NHRI), Taiwan [NHRI-EX104-10437SI to Y.-S.H.]. Funding for open access charge: Academia Sinica, MoST [MoST-103-2321 to W.-H.L.].
Conflict of interest statement. None declared.

REFERENCES

1. Malhotra,J.D. and Kaufman,R.J. (2007) Endoplasmic reticulum stress and oxidative stress: a vicious cycle or a double-edged sword? *Antioxid. Redox Signal.*, **9**, 2277–2293.
2. Holmstrom,K.M. and Finkel,T. (2014) Cellular mechanisms and physiological consequences of redox-dependent signalling. *Nat. Rev. Mol. Cell Biol.*, **15**, 411–421.
3. Tormos,K.V., Anso,E., Hamanaka,R.B., Eisenbart,J., Joseph,J., Kalyanaraman,B. and Chandel,N.S. (2011) Mitochondrial complex III ROS regulate adipocyte differentiation. *Cell Metab.*, **14**, 537–544.
4. Ali,M.H., Schlidt,S.A., Chandel,N.S., Hynes,K.L., Schumacker,P.T. and Gewertz,B.L. (1999) Endothelial permeability and IL-6 production during hypoxia: role of ROS in signal transduction. *Am. J. Physiol.*, **277**, L1057–L1065.
5. Goldstein,B.J., Mahadev,K., Wu,X., Zhu,L. and Motoshima,H. (2005) Role of insulin-induced reactive oxygen species in the insulin signaling pathway. *Antioxid. Redox Signal.*, **7**, 1021–1031.
6. Kumar,B., Koul,S., Khandrika,L., Meacham,R.B. and Koul,H.K. (2008) Oxidative stress is inherent in prostate cancer cells and is required for aggressive phenotype. *Cancer Res.*, **68**, 1777–1785.
7. Rascon,B. and Harrison,J.F. (2010) Lifespan and oxidative stress show a non-linear response to atmospheric oxygen in Drosophila. *J. Exp. Biol.*, **213**, 3441–3448.
8. D'Autreaux,B. and Toledano,M.B. (2007) ROS as signalling molecules: mechanisms that generate specificity in ROS homeostasis. *Nat. Rev. Mol. Cell Biol.*, **8**, 813–824.
9. Rhee,S.G., Kang,S.W., Jeong,W., Chang,T.S., Yang,K.S. and Woo,H.A. (2005) Intracellular messenger function of hydrogen peroxide and its regulation by peroxiredoxins. *Curr. Opin. Cell Biol.*, **17**, 183–189.
10. Scherz-Shouval,R. and Elazar,Z. (2007) ROS, mitochondria and the regulation of autophagy. *Trends Cell Biol.*, **17**, 422–427.
11. Toppo,S., Vanin,S., Bosello,V. and Tosatto,S.C. (2008) Evolutionary and structural insights into the multifaceted glutathione peroxidase (Gpx) superfamily. *Antioxid. Redox Signal.*, **10**, 1501–1514.
12. Brigelius-Flohe,R. and Maiorino,M. (2013) Glutathione peroxidases. *Biochim. Biophys. Acta*, **1830**, 3289–3303.
13. Mills,G.C. (1957) Hemoglobin catabolism. I. Glutathione peroxidase, an erythrocyte enzyme which protects hemoglobin from oxidative breakdown. *J. Biol. Chem.*, **229**, 189–197.
14. Ho,Y.S., Magnenat,J.L., Bronson,R.T., Cao,J., Gargano,M., Sugawara,M. and Funk,C.D. (1997) Mice deficient in cellular glutathione peroxidase develop normally and show no increased sensitivity to hyperoxia. *J. Biol. Chem.*, **272**, 16644–16651.
15. Esworthy,R.S., Mann,J.R., Sam,M. and Chu,F.F. (2000) Low glutathione peroxidase activity in Gpx1 knockout mice protects jejunum crypts from gamma-irradiation damage. *Am. J. Physiol. Gastrointest. Liver physiol.*, **279**, G426–G436.
16. Olson,G.E., Whitin,J.C., Hill,K.E., Winfrey,V.P., Motley,A.K., Austin,L.M., Deal,J., Cohen,H.J. and Burk,R.F. (2010) Extracellular glutathione peroxidase (Gpx3) binds specifically to basement membranes of mouse renal cortex tubule cells. *Am. J. Physiol. Renal Physiol.*, **298**, F1244–F1253.
17. Schneider,M., Forster,H., Boersma,A., Seiler,A., Wehnes,H., Sinowatz,F., Neumuller,C., Deutsch,M.J., Walch,A., Hrabe de Angelis,M. *et al.* (2009) Mitochondrial glutathione peroxidase 4 disruption causes male infertility. *FASEB J.*, **23**, 3233–3242.
18. Chabory,E., Damon,C., Lenoir,A., Kauselmann,G., Kern,H., Zevnik,B., Garrel,C., Saez,F., Cadet,R., Henry-Berger,J. *et al.* (2009) Epididymis seleno-independent glutathione peroxidase 5 maintains sperm DNA integrity in mice. *The Journal of clinical investigation*, **119**, 2074–2085.
19. Wei,P.C., Hsieh,Y.H., Su,M.I., Jiang,X., Hsu,P.H., Lo,W.T., Weng,J.Y., Jeng,Y.M., Wang,J.M., Chen,P.L. *et al.* (2012) Loss of the oxidative stress sensor NPGPx compromises GRP78 chaperone activity and induces systemic disease. *Mol. Cell*, **48**, 747–759.
20. Chang,Y.C., Yu,Y.H., Shew,J.Y., Lee,W.J., Hwang,J.J., Chen,Y.H., Chen,Y.R., Wei,P.C., Chuang,L.M. and Lee,W.H. (2013) Deficiency of NPGPx, an oxidative stress sensor, leads to obesity in mice and human. *EMBO Mol. Med.*, **5**, 1165–1179.
21. Nguyen,V.D., Saaranen,M.J., Karala,A.R., Lappi,A.K., Wang,L., Raykhel,I.B., Alanen,H.I., Salo,K.E., Wang,C.C. and Ruddock,L.W. (2011) Two endoplasmic reticulum PDI peroxidases increase the efficiency of the use of peroxide during disulfide bond formation. *J. Mol. Biol.*, **406**, 503–515.
22. Utomo,A., Jiang,X., Furuta,S., Yun,J., Levin,D.S., Wang,Y.C., Desai,K.V., Green,J.E., Chen,P.L. and Lee,W.H. (2004) Identification of a novel putative non-selenocysteine containing phospholipid hydroperoxide glutathione peroxidase (NPGPx) essential for alleviating oxidative stress generated from polyunsaturated fatty acids in breast cancer cells. *J. Biol. Chem.*, **279**, 43522–43529.
23. Wei,P.C., Lo,W.T., Su,M.I., Shew,J.Y. and Lee,W.H. (2012) Non-targeting siRNA induces NPGPx expression to cooperate with exoribonuclease XRN2 for releasing the stress. *Nucleic Acids Res.*, **40**, 323–332.
24. Peng,D., Hu,T., Soutto,M., Belkhiri,A., Zaika,A. and El-Rifai,W. (2014) Glutathione peroxidase 7 has potential tumour suppressor functions that are silenced by location-specific methylation in oesophageal adenocarcinoma. *Gut*, **63**, 540–551.
25. Wang,L., Zhang,L., Niu,Y., Sitia,R. and Wang,C.C. (2014) Glutathione peroxidase 7 utilizes hydrogen peroxide generated by

Ero1alpha to promote oxidative protein folding. *Antioxid. Redox Signal.*, **20**, 545–556.
26. Peng,D., Belkhiri,A., Hu,T., Chaturvedi,R., Asim,M., Wilson,K.T., Zaika,A. and El-Rifai,W. (2012) Glutathione peroxidase 7 protects against oxidative DNA damage in oesophageal cells. *Gut*, **61**, 1250–1260.
27. Yee Koh,M., Spivak-Kroizman,T.R. and Powis,G. (2008) HIF-1 regulation: not so easy come, easy go. *Trends Biochem. Sci.*, **33**, 526–534.
28. Majmundar,A.J., Wong,W.J. and Simon,M.C. (2010) Hypoxia-inducible factors and the response to hypoxic stress. *Mol. Cell*, **40**, 294–309.
29. Taie,S., Ono,J., Iwanaga,Y., Tomita,S., Asaga,T., Chujo,K. and Ueki,M. (2009) Hypoxia-inducible factor-1 alpha has a key role in hypoxic preconditioning. *J. Clin. Neurosci.*, **16**, 1056–1060.
30. Chen,P.J. and Huang,Y.S. (2012) CPEB2-eEF2 interaction impedes HIF-1alpha RNA translation. *EMBO J.*, **31**, 959–971.
31. Galban,S., Kuwano,Y., Pullmann,R. Jr, Martindale,J.L., Kim,H.H., Lal,A., Abdelmohsen,K., Yang,X., Dang,Y., Liu,J.O. *et al.* (2008) RNA-binding proteins HuR and PTB promote the translation of hypoxia-inducible factor 1alpha. *Mol. Cell. Biol.*, **28**, 93–107.
32. Hagele,S., Kuhn,U., Boning,M. and Katschinski,D.M. (2009) Cytoplasmic polyadenylation-element-binding protein (CPEB)1 and 2 bind to the HIF-1alpha mRNA 3′-UTR and modulate HIF-1alpha protein expression. *Biochem. J.*, **417**, 235–246.
33. Zheng,L., Pan,H., Li,S., Flesken-Nikitin,A., Chen,P.L., Boyer,T.G. and Lee,W.H. (2000) Sequence-specific transcriptional corepressor function for BRCA1 through a novel zinc finger protein, ZBRK1. *Mol. Cell*, **6**, 757–768.
34. Chang,P.H., Hwang-Verslues,W.W., Chang,Y.C., Chen,C.C., Hsiao,M., Jeng,Y.M., Chang,K.J., Lee,E.Y., Shew,J.Y. and Lee,W.H. (2012) Activation of Robo1 signaling of breast cancer cells by Slit2 from stromal fibroblast restrains tumorigenesis via blocking PI3K/Akt/beta-catenin pathway. *Cancer Res.*, **72**, 4652–4661.
35. Marblestone,J.G., Edavettal,S.C., Lim,Y., Lim,P., Zuo,X. and Butt,T.R. (2006) Comparison of SUMO fusion technology with traditional gene fusion systems: enhanced expression and solubility with SUMO. *Protein Sci.*, **15**, 182–189.
36. Huang,Y.S., Kan,M.C., Lin,C.L. and Richter,J.D. (2006) CPEB3 and CPEB4 in neurons: analysis of RNA-binding specificity and translational control of AMPA receptor GluR2 mRNA. *EMBO J.*, **25**, 4865–4876.
37. Hafner,M., Landthaler,M., Burger,L., Khorshid,M., Hausser,J., Berninger,P., Rothballer,A., Ascano,M. Jr, Jungkamp,A.C., Munschauer,M. *et al.* (2010) Transcriptome-wide identification of RNA-binding protein and microRNA target sites by PAR-CLIP. *Cell*, **141**, 129–141.
38. Afroz,T., Skrisovska,L., Belloc,E., Guillen-Boixet,J., Mendez,R. and Allain,F.H. (2014) A fly trap mechanism provides sequence-specific RNA recognition by CPEB proteins. *Genes Dev.*, **28**, 1498–1514.
39. Schelhorn,C., Gordon,J.M., Ruiz,L., Alguacil,J., Pedroso,E. and Macias,M.J. (2014) RNA recognition and self-association of CPEB4 is mediated by its tandem RRM domains. *Nucleic Acids Res.*, **42**, 10185–10195.
40. Iyer,N.V., Kotch,L.E., Agani,F., Leung,S.W., Laughner,E., Wenger,R.H., Gassmann,M., Gearhart,J.D., Lawler,A.M., Yu,A.Y. *et al.* (1998) Cellular and developmental control of O2 homeostasis by hypoxia-inducible factor 1 alpha. *Genes Dev.*, **12**, 149–162.
41. Ryan,H.E., Lo,J. and Johnson,R.S. (1998) HIF-1 alpha is required for solid tumor formation and embryonic vascularization. *EMBO J.*, **17**, 3005–3015.
42. Seagroves,T.N., Ryan,H.E., Lu,H., Wouters,B.G., Knapp,M., Thibault,P., Laderoute,K. and Johnson,R.S. (2001) Transcription factor HIF-1 is a necessary mediator of the pasteur effect in mammalian cells. *Mol. Cell. Biol.*, **21**, 3436–3444.
43. Brocato,J., Chervona,Y. and Costa,M. (2014) Molecular responses to hypoxia-inducible factor 1alpha and beyond. *Mol. Pharmacol.*, **85**, 651–657.
44. Keith,B. and Simon,M.C. (2007) Hypoxia-inducible factors, stem cells, and cancer. *Cell*, **129**, 465–472.
45. Kim,J.W., Evans,C., Weidemann,A., Takeda,N., Lee,Y.S., Stockmann,C., Branco-Price,C., Brandberg,F., Leone,G., Ostrowski,M.C. *et al.* (2012) Loss of fibroblast HIF-1alpha accelerates tumorigenesis. *Cancer Res.*, **72**, 3187–3195.
46. Peng,D.F., Hu,T.L., Soutto,M., Belkhiri,A. and El-Rifai,W. (2014) Loss of glutathione peroxidase 7 promotes TNF-alpha-induced NF-kappaB activation in Barrett's carcinogenesis. *Carcinogenesis*, **35**, 1620–1628.
47. Peng,D.F., Hu,T.L., Soutto,M., Belkhiri,A. and El-Rifai,W. (2014) Glutathione peroxidase 7 suppresses bile salt-induced expression of pro-inflammatory cytokines in Barrett's carcinogenesis. *J. Cancer*, **5**, 510–517.
48. Cohen,T.J., Hwang,A.W., Unger,T., Trojanowski,J.Q. and Lee,V.M. (2012) Redox signalling directly regulates TDP-43 via cysteine oxidation and disulphide cross-linking. *EMBO J.*, **31**, 1241–1252.
49. Benoit,R. and Auer,M. (2011) A direct way of redox sensing. *RNA Biol.*, **8**, 18–23.
50. Zumbrennen,K.B., Wallander,M.L., Romney,S.J. and Leibold,E.A. (2009) Cysteine oxidation regulates the RNA-binding activity of iron regulatory protein 2. *Mol. Cell. Biol.*, **29**, 2219–2229.
51. Fong,C.L., Lentz,A. and Mayfield,S.P. (2000) Disulfide bond formation between RNA binding domains is used to regulate mRNA binding activity of the chloroplast poly(A)-binding protein. *J. Biol. Chem.*, **275**, 8275–8278.
52. Benoit,R.M., Meisner,N.C., Kallen,J., Graff,P., Hemmig,R., Cebe,R., Ostermeier,C., Widmer,H. and Auer,M. (2010) The x-ray crystal structure of the first RNA recognition motif and site-directed mutagenesis suggest a possible HuR redox sensing mechanism. *J. Mol. Biol.*, **397**, 1231–1244.
53. Wang,C.F. and Huang,Y.S. (2012) Calpain 2 activated through N-methyl-D-aspartic acid receptor signaling cleaves CPEB3 and abrogates CPEB3-repressed translation in neurons. *Mol. Cell. Biol.*, **32**, 3321–3332.
54. Pavlopoulos,E., Trifilieff,P., Chevaleyre,V., Fioriti,L., Zairis,S., Pagano,A., Malleret,G. and Kandel,E.R. (2011) Neuralized1 activates CPEB3: a function for nonproteolytic ubiquitin in synaptic plasticity and memory storage. *Cell*, **147**, 1369–1383.
55. Igea,A. and Mendez,R. (2010) Meiosis requires a translational positive loop where CPEB1 ensues its replacement by CPEB4. *EMBO J.*, **29**, 2182–2193.
56. Ortiz-Zapater,E., Pineda,D., Martinez-Bosch,N., Fernandez-Miranda,G., Iglesias,M., Alameda,F., Moreno,M., Eliscovich,C., Eyras,E., Real,F.X. *et al.* (2012) Key contribution of CPEB4-mediated translational control to cancer progression. *Nat. Med.*, **18**, 83–90.
57. Berger-Sweeney,J., Zearfoss,N.R. and Richter,J.D. (2006) Reduced extinction of hippocampal-dependent memories in CPEB knockout mice. *Learn Mem.*, **13**, 4–7.
58. Chao,H.W., Tsai,L.Y., Lu,Y.L., Lin,P.Y., Huang,W.H., Chou,H.J., Lu,W.H., Lin,H.C., Lee,P.T. and Huang,Y.S. (2013) Deletion of CPEB3 enhances hippocampus-dependent memory via increasing expressions of PSD95 and NMDA receptors. *J. Neurosci.*, **33**, 17008–17022.
59. Tsai,L.Y., Chang,Y.W., Lin,P.Y., Chou,H.J., Liu,T.J., Lee,P.T., Huang,W.H., Tsou,Y.L. and Huang,Y.S. (2013) CPEB4 knockout mice exhibit normal hippocampus-related synaptic plasticity and memory. *PLoS One*, **8**, e84978.
60. Okazaki,S., Tachibana,T., Naganuma,A., Mano,N. and Kuge,S. (2007) Multistep disulfide bond formation in Yap1 is required for sensing and transduction of H2O2 stress signal. *Mol. Cell*, **27**, 675–688.
61. Hake,L.E., Mendez,R. and Richter,J.D. (1998) Specificity of RNA binding by CPEB: requirement for RNA recognition motifs and a novel zinc finger. *Mol. Cell. Biol.*, **18**, 685–693.
62. Merkel,D.J., Wells,S.B., Hilburn,B.C., Elazzouzi,F., Perez-Alvarado,G.C. and Lee,B.M. (2013) The C-terminal region of cytoplasmic polyadenylation element binding protein is a ZZ domain with potential for protein-protein interactions. *J. Mol. Biol.*, **425**, 2015–2026.